Anion-Cation-Anion Ion Triplet Characterization by Computation and Photoelectron Spectroscopy

Journal:	*The Journal of Organic Chemistry*
Manuscript ID	jo-2024-02392k
Manuscript Type:	Article
Date Submitted by the Author:	24-Sep-2024
Complete List of Authors:	Cao, Wenjin; Pacific Northwest National Laboratory, Physical Sciences Division Wang, Xue-Bin; Pacific Northwest National Laboratory, Chemical & Materials Scienecs Division Kass, Steven; University of Minnesota Twin Cities, Department of Chemistry

Anion-Cation-Anion Ion Triplet Characterization by Computation and Photoelectron Spectroscopy

Wenjin Cao,[2] Xue-Bin Wang,[2,*] Steven R. Kass[1,*]

[1]Department of Chemistry, University of Minnesota

207 Pleasant Street SE, Minneapolis, Minnesota 55455, USA

[2]Physical Sciences Division, Pacific Northwest National Laboratory, Richland, Washington 99352, USA

E-mail: xuebin.wang@pnnl.gov, kass@umn.edu

ABSTRACT

Ion triplets of the chloride salts of two commonly used weakly coordinating cations are reported (i.e., $Cl^- \cdot NMe_4^+ Cl^-$ (**1**$^-$) and $Cl^- \cdot PPh_4^+ Cl^-$ (**2**$^-$)). Negative ion photoelectron spectra at 20 K afford vertical and adiabatic detachment energies of 5.18 and 5.00 eV (**1**$^-$) and 5.03 and 4.70 eV (**2**$^-$), respectively. These results are well reproduced by CCSD(T) calculations whereas M06-2X is systematically too small by ~0.3 eV (i.e., 7 kcal mol^{-1}). The structures of both **1**$^-$ and **2**$^-$ have five or six C–H•••Cl$^-$ interactions that stabilize these cluster anions by 32 (**1**$^-$) and 27 (**2**$^-$) kcal mol^{-1} as given by their chloride dissociation enthalpies. These values drop to 7.4 and 3.8 kcal mol^{-1} in dichloromethane based up conductor-like polarizable continuum model calculations and suggest that $X^- \cdot M^+ X^-$ ion triplets with a weakly coordinating cation maybe the reactive form of salts under some conditions.

INTRODUCTION

Incorporation of positively and negatively charged substituents into otherwise noncharged catalytic platforms when paired with weakly coordinating counterions afford salts that display enhanced catalytic activity in nonpolar media.[1-22] The structures of these catalysts, and ionic intermediates in general, presumably afford ion pairs and higher-order aggregates in commonly used solvents with low dielectric constants such as chloroform ($\varepsilon = 4.71$), dichloromethane (8.93), diethyl ether (4.24), tetrahydrofuran (7.43), and toluene (2.37).[23] "Free" ions and ion triplets (i.e., $X^- \cdot M^+ X^-$ and $M^+ \cdot X^- M^+$) are also expected to be present but relatively little is known about the reactivities and structures of the latter species when M^+ is an organic ion. To begin to probe these species, computations and negative ion photoelectron spectroscopy (NIPES) studies of the chloride salts of tetramethylammonium and tetraphenylphosphonium ions (i.e., $Cl^- \cdot NMe_4^+ Cl^-$ (**1**$^-$) and $Cl^- \cdot PPh_4^+ Cl^-$ (**2**$^-$)) were investigated. These cations were chosen because they are commonly considered to be weakly coordinating and as a result are used in numerous chemical applications.[24]

METHODS

Experiments. Ion clusters **1**$^-$ and **2**$^-$ were generated by electrospray ionization of ~0.1 mM solutions of $NMe_4^+ Cl^-$ in 1:3 H_2O/CH_3CN and $PPh_4^+ Cl^-$ in CH_3CN, respectively. The resulting anions were accumulated for 20 – 100 ms in the cryogenic 3D ion trap of an instrument that previously has been described.[25] After collisional cooling to 20 K with helium buffer gas the negative ions were pulsed into a time-of-flight mass spectrometer at 10 Hz, and the desired ion-triplets were mass-selected and decelerated for photodetachment at 157 nm (7.866 eV) with a Lambda Physik CompexPro F2 laser operated at 20 Hz. Photoelectron spectra were recorded alternately with the ion beam on and off to obtain shot-to-shot background corrected spectra. The observed electron flight times were converted to kinetic energies using the known spectrum of I^-

/$Au(CN)_2^-$ as a calibrant.[26,27] Vertical detachment energies (VDEs) were obtained from the peak maxima and the adiabatic detachment energies (ADEs) were assigned using a linear fit of the onset region. The energy resolution ($\Delta E/E$) is estimated to be ~2% or 20 meV at 1 eV and the uncertainties in the VDEs and ADEs are approximately 0.1 eV.

Computations. Initial geometries were obtained by adding Cl^- at different locations to previously reported structures for NMe_4^+ Cl^- and PPh_4^+ Cl^-[24] and then full optimizations were carried out using the M06-2X[28-30] hybrid density functional and the aug-cc-pVDZ basis set.[31] Vibrational frequencies were computed to ensure that each located stationary point corresponds to an energy minimum (i.e., only has positive eigenvalues) and to obtain the zero-point energies (ZPEs). Single point energies were computed subsequently with the larger aug-cc-pVTZ basis set and the same density functional. For the smaller system (i.e., $Cl^- \cdot NMe_4^+$ Cl^- and related species) M06-2X/aug-cc-pVTZ and wB97xD/aug-cc-pVDZ optimizations, and wB97xD/aug-cc-pVTZ// wB97xD/aug-cc-pVDZ, M06-2X/aug-cc-pVQZ//M06-2X/aug-cc-pVDZ, and CCSD(T)/aug-cc-pVTZ//M06-2X/aug-cc-pVDZ energies were also obtained.[32-34] For the larger tetraphenylphosphonium ion containing species, M06-2X/aug-cc-pVTZ single point energies were computed. VDEs and ADEs at 0 K were subsequently derived from the energy differences between the anions and their corresponding radicals, where the fully optimized geometries for the latter structures were used for the ADEs and the anion geometries were employed to obtain the VDEs. Conductor-like polarizable continuum model (CPCM)[35,36] single point energies on M06-2X/aug-cc-pVDZ optimized structures with the M06-2X/aug-cc-pVTZ basis set were also carried out on Cl^-•••HCl, $Cl^- \cdot NMe_4^+$ Cl^-, $Cl^- \cdot PPh_4^+$ Cl^-, and their constituents. All these calculations were carried out using Gaussian 16[23] either at the Minnesota Supercomputer Institute for Advanced Computational Research or on an iMac computer with the use of Gaussview 6.[37] Moreover,

Franck-Condon and density-of-state (DOS) simulations were also carried out for selected species to simulate spectra to compare with experimental ones. The Franck-Condon simulations were performed with the ezSpectrum program,[38] while the DOS simulations were done with the Multiwfn software package.[39]

RESULTS AND DISCUSSION

Negative ion photoelectron spectra of $Cl^- \cdot NMe_4^+ Cl^-$ and $Cl^- \cdot PPh_4^+ Cl^-$ were obtained at 20 K and are shown in Figure 1. Both spectra consist of a partially resolved broad band approximately

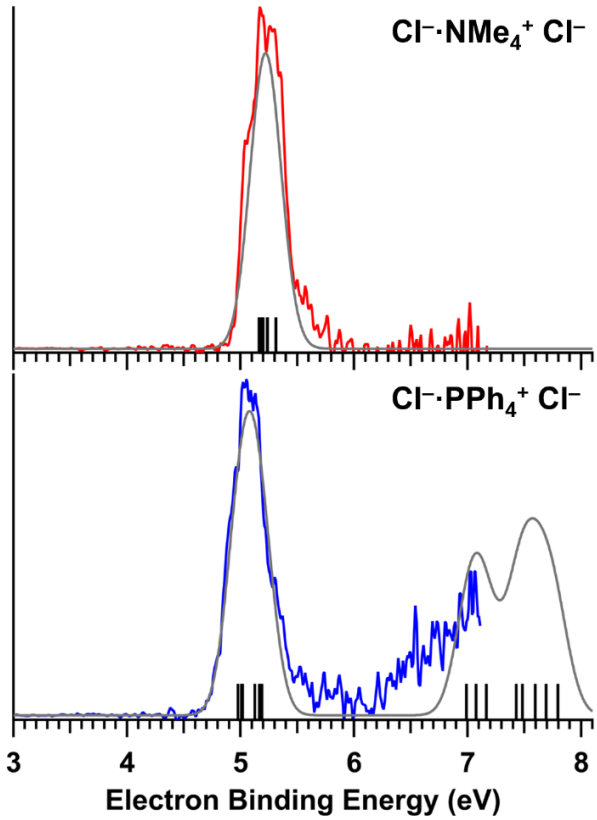

Figure 1. NIPE spectra of $Cl^- \cdot NMe_4^+ Cl^-$ (in red) and $Cl^- \cdot PPh_4^+ Cl^-$ (in blue) recorded at 20 K with a 157 nm laser, and their comparisons to simulated density of state (DOS) spectra (in gray) convoluted based on computed relative energies of frontier molecular orbitals (MOs, black sticks) using gaussians with 0.2 eV full width at half maximum for each stick. See Figure S1 for rendered MOs.

1 eV in width with peak maxima corresponding to the VDEs of 5.18 ± 0.10 and 5.03 ± 0.10 eV, respectively. Poorly resolved features are observed at lower and higher energies than the band maxima, in part, due to the 0.109 eV spin-orbit coupling of chlorine atom.[40] A linear fit of the rising portion of the onset regions of the spectra provide an upper bound estimate for the ADEs of $Cl^- \cdot NMe_4^+ Cl^-$ and $Cl^- \cdot PPh_4^+ Cl^-$ of 5.00 ± 0.10 and 4.70 ± 0.10 eV, respectively. These values are 1.39 and 1.09 eV or 32.1 and 25.1 kcal mol^{-1}, respectively larger than the previously reported ADE for Cl^- of 3.613577 ± 0.000044 eV.[41] In addition, there are some extra features at higher EBEs close to the photon energy limit for the $Cl^- \cdot PPh_4^+ Cl^-$ complex, leading to a gradually rising tail (6.5 – 7.2 eV) (Figure 1). Such a feature is not present for the $Cl^- \cdot NMe_4^+ Cl^-$ complex whose NIPE spectrum exhibits a flat profile on the higher EBE side of the main band.

$Cl^- \cdot NMe_4^+ Cl^-$. M06-2X/aug-cc-pVDZ structures for $Cl^- \cdot NMe_4^+ Cl^-$ were located by starting with a previously optimized geometry for $NMe_4^+ Cl^-$ and adding Cl^- at several different locations.[24] The most favorable species has C_S symmetry and is nearly C_{2V} ($\mathbf{1}^-_{C_S}$) whereas its C_{3V} analog ($\mathbf{1}^-_{C_{3V}}$) is 5.0 – 5.5 kcal mol^{-1} less stable depending upon the computational method and basis set employed (Table 1, Figure 2, and the supporting information for more details). In both structures there are six C–H•••Cl^- interactions with distances of 2.33 and 2.63 Å in $\mathbf{1}^-_{C_S}$ and longer lengths of 2.47 and 2.83 Å in the less stable isomer (i.e., $\mathbf{1}^-_{C_{3V}}$).

Upon loss of an electron from $\mathbf{1}^-_{C_S}$ and $\mathbf{1}^-_{C_{3V}}$ there is little change to the structure of the tetramethylammonium cation core but the symmetries of the respective clusters increase to C_{2V} and decrease to C_S. Significant changes in the C–H•••Cl^- distances are observed and for $\mathbf{1}^{\bullet}_{C_{2V}}$ there is a 0.14 Å contraction of four of the C–H•••Cl interactions and a 0.18 Å elongation of the other two. In contrast, for $\mathbf{1}^{\bullet}_{C_S}$ there is a reduction of 0.11 Å in of the C–H•••Cl distances involving the three

Table 1. Experimental and Calculated VDEs, ADEs, and Fragmentation Energies of $Cl^- \cdot NMe_4^+$ Cl^- ($\mathbf{1}^-_{Cs}$ and $\mathbf{1}^-_{C3V}$) and $Cl^- \cdot PPh_4^+$ Cl^- ($\mathbf{2}^-$).[a]

cmpd	quantity	M06-2X	CCSD(T)	expt
$\mathbf{1}^-_{Cs}$	VDE (eV)	4.83	5.11	5.18 ± 0.10
	ADE (eV)	4.78	5.06	5.00 ± 0.10
	ΔH°_{Diss}(anion)[b]	32.1	32.3	~32.0[c]
	ΔH°_{Diss}(radical)[b]	5.8	-3.6	
$\mathbf{1}^-_{C3V}$	VDE (eV)	4.88	4.75	
	ADE (eV)	4.77	4.62	
	ΔH°_{Diss}(anion)[b]	27.1	26.8	
	ΔH°_{Diss}(radical)[b]	1.0	1.2	
$\mathbf{2}^-$	VDE (eV)	4.78	5.06[d]	5.03 ± 0.10
	ADE (eV)	4.38	4.66[d]	4.70 ± 0.10
	ΔH°_{Diss}(anion)[b]	25.9		~25.1[c]
	ΔH°_{Diss}(radical)[b]	8.8		

[a]M06-2X = M06-2X/aug-cc-pVTZ//M06-2X/aug-cc-pVDZ and CCSD(T) = CCSD(T)/aug-cc-pVTZ//M06-2X/aug-cc-pVDZ. [b]Fragmentation energies of Cl^- and $Cl^\bullet$ (ΔH°_{Diss}) are in kcal mol^{-1}. [c]Expt ADE(ion triplet) – ADE(Cl^-). [d]Estimated VDE and ADE CCSD(T) energies for $\mathbf{2}^-$ as indicated in the text.

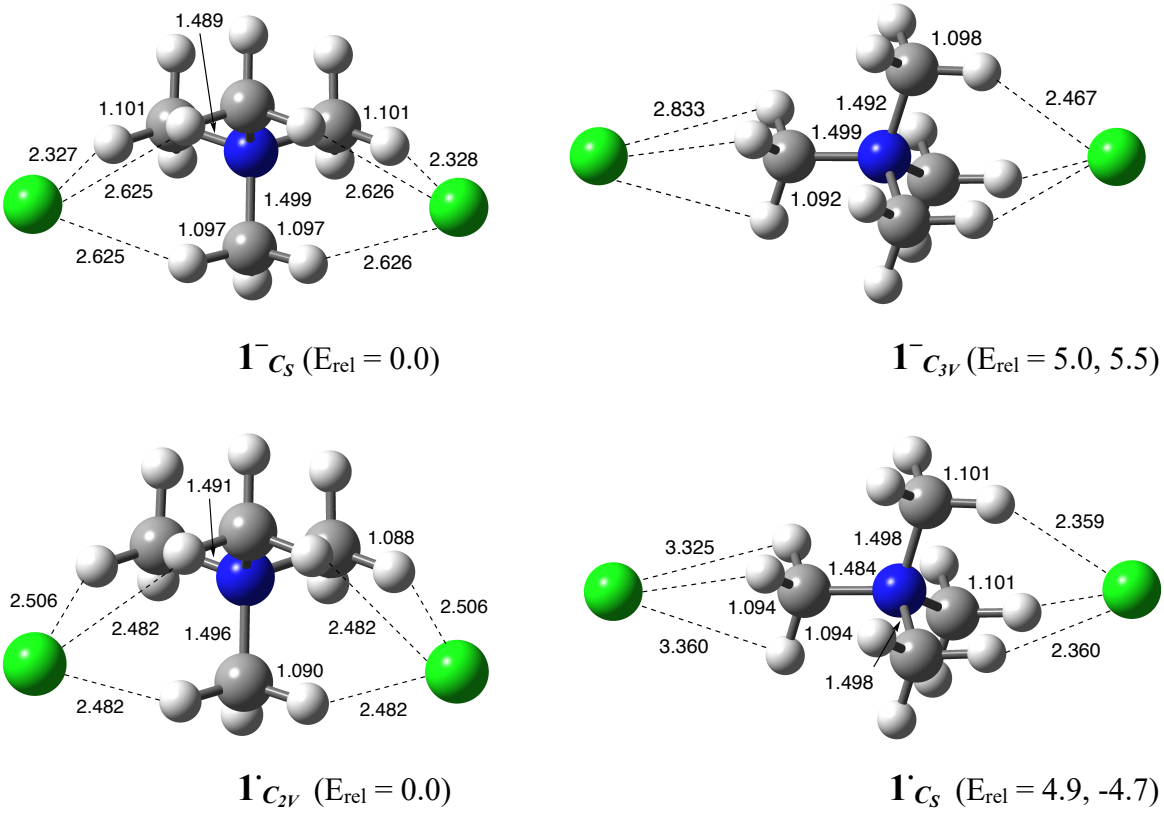

$\mathbf{1}^-_{Cs}$ (E_{rel} = 0.0) $\mathbf{1}^-_{C3V}$ (E_{rel} = 5.0, 5.5)

$\mathbf{1}^\bullet_{C2V}$ (E_{rel} = 0.0) $\mathbf{1}^\bullet_{Cs}$ (E_{rel} = 4.9, -4.7)

Figure 2. Optimized M06-2X/aug-cc-pVDZ structures of $Cl^- \cdot NMe_4^+$ Cl^- with C_S (top left) and C_{3V} (top right) symmetry and their corresponding radicals (bottom row, $\mathbf{1}^\bullet_{C2V}$ (left) and $\mathbf{1}^\bullet_{Cs}$ (right)), where bond distances are given in Angstroms and the respective M06-2X and CCSD(T) relative energies are given in kcal mol^{-1}.

single hydrogen bond donating methyl groups and large increases of 0.49 and 0.53 Å for the three C–H•••Cl interactions to the single methyl group. In this latter structure the computed atomic polarization tensor (APT)[42] charges and Mulliken spin densities are smallest and largest, respectively on the latter chlorine (i.e., q = 0.01 vs -0.95 and 1.00 vs 0.00 e^-). It is thus the predicted site for photoelectron detachment and the primary location where the unpaired electron resides. For $\mathbf{1}^{\bullet}_{C_{2V}}$, APT charges and Mulliken spin densities are equivalent on the two Cl atoms (i.e., q = -0.14 and 0.49 e^-, respectively), indicating photodetachment occurs across the two Cl atoms, which is supported by highest occupied molecular orbital (HOMO) of $\mathbf{1}^-_{C_S}$ with electron clouds uniformly distributed across the two Cl atoms (Figure S1).

Despite some changes in the molecular geometries upon photodetachment, the simulated Franck-Condon spectrum based on the $\mathbf{1}^{\bullet}_{C_{2V}} \leftarrow \mathbf{1}^-_{C_S}$ transition exhibits a narrow-band spectral profile consisting of mainly one set of transitions attributed to the Cl scissoring mode with a band width (~100 meV full width at half maximum) substantially narrower compared to that of the experimental NIPE spectrum (Figure S2). On the other hand, due to the presence of two Cl^- ions, there are a number of close-lying molecular orbitals (MOs) beneath the HOMO. As shown in Figure 1 and Figure S1, there are six MOs within an energy window of 0.15 eV that correspond to the six 3p orbitals of the two Cl^- anions, followed by deeper MOs that are attributed to the NMe_4^+ moiety. Transitions arising from these close-lying MOs cause band broadening, which is nicely reproduced by a density of state (DOS) simulation as seen from Figure 1. Given the large energy gap of > 5 eV between the MOs dominated by the two Cl^- ions and those mainly attributed to the NMe_4^+ moiety (Figure S2), no additional transitions are experimentally observed due to the photon energy limit at 157 nm of 7.866 eV.

In terms of the energetics, the CCSD(T)/aug-cc-pVTZ//M06-2X/aug-cc-pVDZ (referred to as CCSD(T) hereafter) predictions for the VDE and ADE are in excellent accord with the experimental results (i.e., VDE = 5.11 (CCSD(T)) vs 5.18 ± 0.10 (expt) and ADE = 5.06 (CCSD(T)) vs 5.00 ± 0.10 eV (expt)). In contrast, the M06-2X/aug-cc-pVTZ//M06-2X/aug-cc-pVDZ (referred to as M06-2X hereafter) calculated VDE and ADE are smaller than the experimental values by 0.35 and 0.22 eV, respectively. To assess these respective 8.1 and 5.1 kcal mol^{-1} differences, the impact of the basis set (aug-pVDZ, aug-pVTZ, and aug-pVQZ), dispersion, and the effect of using optimized aug-cc-pVTZ geometries were investigated. The results of these calculations are provided in the supporting information since the changes in the VDE and ADE are minimal (i.e., ≤ 0.05 eV). In addition, similar results were obtained with the wB97xD hybrid functional.

As anticipated, the computed M06-2X and CCSD(T) chloride ion dissociation enthalpies of the ion triplet $\mathbf{1}^-$ are much larger than the corresponding values for the loss of chlorine atom from $\mathbf{1}^\bullet$. That is, cleavage of $\mathbf{1}^-$ to NMe_4^+ Cl^- and Cl^- is computed to be endothermic by 32.3 (CCSD(T)) and 32.1 (M06-2X) kcal mol^{-1} whereas the separation energy for $\mathbf{1}^\bullet$ to NMe_4^+ Cl^- and $Cl^\bullet$ is -3.6 (CCSD(T)) and 5.8 (M06-2X) kcal mol^{-1}. As a result, the predicted ADE of $\mathbf{1}^-$ is 33.4 (CCSD(T)) and 26.9 (M06-2X) kcal mol^{-1} larger than for the experimental ADE of Cl^- (i.e., 3.613 eV).[39] This is in excellent accord with the measured difference of 1.39 ± 0.10 eV (32.1 ± 2.3 kcal mol^{-1}) and is similar to ΔADE (Cl–H•••Cl^- – Cl^-) = 1.28 eV (29.5 kcal mol^{-1}).[43]

Cl^- · PPh_4^+ Cl^-. Chloride anion was added to a previously optimized structure for PPh_4^+ Cl^- at a few different positions and the most favorable M06-2X/aug-cc-pVDZ geometry was found to have C_S symmetry ($\mathbf{2}^-$, Figure 3). Two phenyl rings interact with both chloride ions via their ortho hydrogens to the phosphorous atom resulting in four C–H•••Cl^- interactions with distances of 2.45

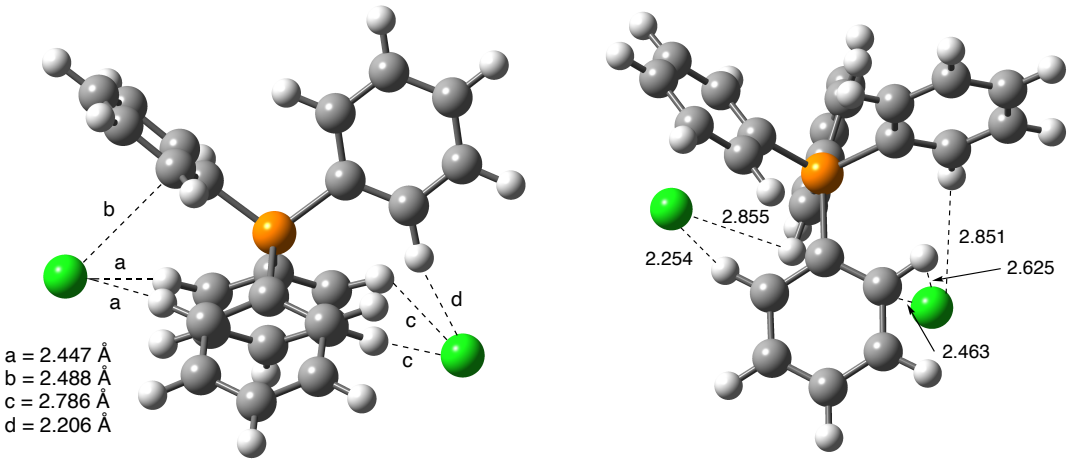

Figure 3. Optimized M06-2X/aug-cc-pVDZ structures of $Cl^- \cdot PPh_4^+$ Cl^- (**2**$^-$) with C_S symmetry (left) and its corresponding C_1 radical (**2**$^{\bullet}$ (right)), where Cl•••H (a, c, d and specified lengths) and Cl•••ring plane (b) distances are given in Angstroms; one distance (2.463 Å) in **2**$^{\bullet}$ corresponds to a Cl•••C separation.

and 2.79 Å. A fifth such hydrogen bond to an ortho hydrogen on one of the two remaining phenyl groups has an even shorter length of 2.21 Å. The distance between the ring plane of the last phenyl substituent as defined by the carbon atom bound to phosphorous and its adjacent carbon atoms and one of the chloride ions is 2.49 Å.

Upon electron loss from **2**$^-$ there is a big change in the structure of the tetraphenylphosphonium cation core in that the phenyl rings rotate about the C–P bonds and the C–H•••Cl^- distances elongate and contract by large amounts (i.e., +0.41, +0.65, -0.16, -0.19, and -0.32 Å). These changes are in accord with the observed tail in the onset region of the spectrum as this is indicative of a significant geometry difference between the anion and its corresponding radical. Atomic polarization tensor[42] charges and Mulliken spin densities are quite different for the two chlorine atoms (q = -0.77 vs -0.26 and spin densities of 0.00 and 0.63, respectively) and indicate that the bulk of the spin density

resides on the chlorine on the right side of $\mathbf{2}^{\bullet}$ as shown in Figure 3. This also agrees with computed HOMO of $\mathbf{2}^{-}$ with electrons exclusively located around this Cl atom (Figure S1). Similar to $Cl^- \cdot NMe_4^+$ Cl^-, the M06-2X/aug-cc-pVDZ calculations for $Cl^- \cdot PPh_4^+$ Cl^- also predict a series of close-lying MOs with the electrons mainly located on the Cl atoms but with a much smaller energy gap of ~1.8 eV to those primarily located on the PPh_4^+ group (Figure S1). As the result, the transitions from ionizing these PPh_4^+ MOs are also present in the experimental NIPE spectrum and appear as the rising tail from EBE = 6.5 – 7.2 eV. Due to the large geometric changes that occur upon photodetachment, we were unable to simulate a Franck-Condon spectrum for this species but the DOS simulation is in good agreement with the experimental NIPE spectrum (Figure 1).

Given the relatively large size of Ph_4P^+, CCSD(T) calculations with the aug-cc-pVTZ basis set are impractical for $\mathbf{2}^{-}$ and $\mathbf{2}^{\bullet}$ with our computational resources. This is unfortunate since this method provides a VDE and ADE for $\mathbf{1}^{-}$ that are in excellent accord with experiment whereas the computationally less demanding M06-2X calculations give poorer results. However, since it is much easier to reliably compute relative energies than absolute values, an estimated CCSD(T) VDE and ADE for $\mathbf{2}^{-}$ was determined as illustrated for the latter case in equation 1. This affords predictions of 4.66 and 5.06 eV for the ADE and VDE of $\mathbf{2}^{-}$ which are in excellent accord with the experimental results of 4.70 ± 0.10 and 5.03 ± 0.10 eV, respectively.

$$\mathrm{ADE}(\mathbf{1}^-)_{\mathrm{M06\text{-}2X}} - \mathrm{ADE}(\mathbf{2}^-)_{\mathrm{M06\text{-}2X}} \approx \mathrm{ADE}(\mathbf{1}^-)_{\mathrm{CCSD(T)}} - \mathrm{ADE}(\mathbf{2}^-)_{\mathrm{CCSD(T)}} \quad (1)$$

$$4.78 - 4.38 \text{ eV} = 5.06 - \mathrm{ADE}(\mathbf{2}^-)_{\mathrm{CCSD(T)}} \text{ eV}$$

$$\mathrm{ADE}(\mathbf{2}^-)_{\mathrm{CCSD(T)}} = 4.66 \text{ eV}$$

Given that Ph_4P^+ is a more weakly coordinating cation than NMe_4^+, it is not surprising that the M06-2X fragmentation energy of Cl^- from $\mathbf{2}^{-}$ is less than for $\mathbf{1}^{-}$ (i.e., 25.9 vs 32.1 kcal mol^{-1}) and

that its observed ADE is smaller (4.70 vs 5.00 eV) and only 1.09 eV (25.1 kcal mol^{-1}) larger than for Cl^-. This former result is similar to the 26 and 24 kcal mol^{-1} chloride anion clustering energy of phenol and acetic acid, respectively,[44] and indicates that the stabilizing influence of PPh_4^+ Cl^- in the gas phase is similar to neutral hydrogen bond donors with modest acidities. In solution one might expect the clustering abilities of salts to be smaller than their comparable non-charged Brønsted acids in the gas phase. To examine this possibility, conductor-like polarizable continuum model (CPCM)[35,36] computations in dichloromethane were carried out on Cl^-•••HCl, $Cl^- \cdot NMe_4^+$ Cl^-, $Cl^- \cdot PPh_4^+$ Cl^-, and their fragmentation products. As anticipated, the M06-2X gas phase clustering energies dropped from 25.5, 32.1, and 25.9 kcal mol^{-1}, respectively to 10.8, 7.4, and 3.8 kcal mol^{-1}. These results suggest that anion-cation-anion ion triplets especially when the cation is weakly coordinating maybe the reactive form of salts under some conditions.

CONCLUSIONS

Triple ions $Cl^- \cdot NMe_4^+$ Cl^- (**1**$^-$) and $Cl^- \cdot PPh_4^+$ Cl^- (**2**$^-$) were examined at 20 K by negative ion photoelectron spectroscopy and their ADEs are 1.39 and 1.09 eV larger than for Cl^-. These results are well reproduced by CCSD(T) calculations but M06-2X values are systematically too small by ~0.3 eV. The structures of these ion triplets are stabilized by multiple C–H•••Cl^- hydrogen bonds (5 or 6) and a Cl^-–π-bond interaction in **2**$^-$. CPCM calculations indicate that this stabilization is greatly diminished in solution even in a nonpolar solvent and thus ion triplets could be the reactive form of salts in some instances.

ASSOCIATED CONTENT:

Data Availability Statement

The data underlying this study are available in the published article and its Supporting Information.

Supporting Information

Rendered high-lying molecular orbitals; Franck-Condon simulated spectrum; computed energies and xyz coordinates for all of the calculated structures and the complete citation to ref. 23. This material is available free of charge via the internet at http://pubs.acs.org.

AUTHOR INFORMATION

Corresponding Author

*E-mail: kass@umn.edu and xuebin.wang@pnnl.gov.

ORCID

Xue-Bin Wang: 0000-0001-8326-1780
Steven R. Kass: 0000-0001-7007-9322

Notes

The authors declare no competing financial interests.

ACKNOWLEDGMENTS

Generous support from the National Science Foundation (CHE-1955186 and CHE-2346852), the donors of the American Chemical Society Petroleum Research Fund (ACS PRF 65096-ND4) and the Minnesota Supercomputing Institute for Advanced Computational Research are gratefully acknowledged. The photoelectron spectra work was supported by U.S. Department of Energy (DOE), Office of Science, Office of Basic Energy Sciences, Division of Chemical Science, Geosciences, and Biosciences, Condensed Phase and Interfacial Molecular Science program, FWP 16248.

REFERENCES

1. Fan, Y.; Kass, S. R. Electrostatically Enhanced Thioureas. *Org. Lett.* **2016**, *14*, 188–191.
2. Ma, J.; Kass, S. R. Electrostatically Enhanced Phosphoric Acids: A Powerful Tool in Brønsted Acid Catalysis. *Org. Lett.* **2016**, *18*, 5812–5815.
3. Fan, Y.; Kass, S. R. Enantioselective Friedel-Crafts Alkylation between Nitroalkenes and Indoles Catalyzed by Charge Activated Thiourea Organocatalysts. *J. Org. Chem.* **2017**, *82*, 13288–13296.
4. Ma, J.; Kass, S. R. Asymmetric Arylation of 2,2,2-Trifluoroacetophenones Catalyzed by Chiral Electrostatically-Enhanced Phosphoric Acids. *Org. Lett.* **2018**, *20*, 2689–2692.
5. Fan, Y.; Tiffner, M.; Schörgenhumer, J.; Robiette, R.; Waser, M.; Kass, S. R. Synthesis of Cyclic Organic Carbonates Using Atmospheric Pressure CO_2 and Charge-Containing Thiourea Catalysts. *J. Org. Chem.* **2018**, *83*, 9991–10000.
6. Fan, Y.; Payne, C.; Kass, S. R. Quantification of Catalytic Activity for Electrostatically Enhanced Thioureas via Reaction Kinetics and a UV−Vis Spectroscopic Measurement. *J. Org. Chem.* **2018**, *83*, 10855–10863.
7. Ma, J.; Kass. S. R. Electrostatically Enhanced Phosphoric Acids and Their Applications in Asymmetric Friedel-Crafts Alkylations. *J. Org. Chem.* **2019**, *84*, 11125–11134.
8. Riegel, G. F.; Kass, S. R. N-Vinyl and N-Aryl Hydroxypyridinium Ions: Charge-Activated Catalysts with Electron Withdrawing Groups. *J. Org. Chem.* **2020**, *85*, 6017–6026.
9. Payne, C.; Kass, S. R. Structural Considerations for Charge-Enhanced Brønsted Acid Catalysts. *J. Phys. Org. Chem.* **2020**, *33*, e4069 (1–16).

10. Riegel, G. F.; Payne, C.; Kass, S. R. Effects of Brønsted Acid Co-Catalysts on the Activities and Selectivities of Charge-Enhanced Thiourea Organocatalysts in Friedel-Crafts and Oxa-Pictet-Spengler Reactions. *J. Phys. Org. Chem.*, **2022**, *35*, e4321 (1–12).
11. Riegel, G. F.; Takashige, K.; Lovstedt, A.; Kass, S. R. Charge-Activated TADDOLs: Recyclable Organocatalysts for Asymmetric (Hetero-)Diels–Alder Reactions. *J. Phys. Org. Chem.*, **2022**, *35*, e4355 (1–13).
12. Blechschmidt, D. R.; Lovstedt, A.; Kass, S. R. Metallocenium Lewis Acid Catalysts for Use in Friedel-Crafts Alkylation and Diels-Alder Reactions. *Organometallics* **2022**, *41*, 2648–2655.
13. Smajlagic, I.; White, B.; Azeez, O.; Pilkington, M.; Dudding, T. Organocatalysis Linked to Charge-Enhanced Acidity with Superelectrophilic Traits. *ACS Catalysis* **2022**, *12*, 1128–1138.
14. Smajlagic, I.; Guest, M.; Durán, R.; Herrera, B.; Dudding, T. Mechanistic Insight toward Understanding the Role of Charge in Thiourea Organocatalysis. *J. Org. Chem*. **2020**, *85*, 585–593.
15. Chen, L.; Xiao, B.-X.; Du, W.; Chen, Y.-C. Quaternary Phosphonium Salts as Active Brønsted Acid Catalysts for Friedel–Crafts Reactions. *Org. Lett*. **2019**, *21*, 5733–5736.
16. Smajlagic, I.; Durán, R.; Pilkington, M.; Dudding, T. Cyclopropenium Enhanced Thiourea Catalysis. *J. Org. Chem*. **2018**, *83*, 13973–13980.
17. Smajlagic, I.; Carlson, B.; Rosano, N.; Foy, H.; Dudding, T. Charge-Enhanced Thiourea Catalysts as Hydrogen Bond Donors for Friedel–Crafts Alkylations. *Tetrahedron* **2019**, *75*, 130757 (1–7).

18. Anzabi, M. Y.; Yazdani, H.; Bazgir, A. Electrostatically Enhanced Sulfuric Acid: A Strong Brønsted Acidic Catalyst for Multi-Component Reactions. *Catal. Lett*. **2019**, *149,* 1934–1940.

19. Yan, C.-X.; Wu, R.-Z.; Lu, K.; Yang, F.-L.; Yang, X.-S.; Wang, R.; Yang, X.; Zhou, P.-P.; Shao, X. Why Electrostatically Enhanced Thiourea is Better than Schreiner's Thiourea in Both Catalytic Activity and Regioselectivity?. *Org. Chem. Frontiers* **2019**, *6*, 1821–1831.

20. Szczepanik, P. M.; Mikhaylov, A. A.; Hylse, O.; Kučera, R.; Daďová, P.; Nečas, M.; Kubala, L.; Paruch, K.; Švenda, J. Convergent Assembly of the Tricyclic Labdane Core Enables Synthesis of Diverse Forskolin-like Molecules. *Angew. Chem., Int. Ed.* **2023**, *62*, e202213183 (1 of 7).

21. Patel, B.; Dabas, S.; Patel, P.; Subramanian, S. Electrostatically Tuned Phenols: A Scalable Organocatalyst for Transfer Hydrogenation and Tandem Reductive Alkylation of *N*-Hetero-arenes. *Chem. Sci*. **2023**, *14*, 540–549.

22. Rostami, A.; Mahmoodabadi, M.; Ebrahimi, A. H.; Khosravi, H.; Al-Harrasi, A. An Electrostatically Enhanced Phenol as a Simple and Efficient Bifunctional Organocatalyst for Carbon Dioxide Fixation. *ChemSusChem* **2018**, *11*, 4262–4268.

23. Frisch, M. J.; Trucks, G. W.; Schlegel, H. B.; Scuseria, G. E.; Robb, M. A. et al. Gaussian 16; Gaussian, Inc., Wallingford CT, 2016.

24. Dempsey, S. H.; Kass, S. R. Liberating the Anion: Evaluating Weakly Coordinating Cations. *J. Org. Chem.* **2022**, *87*, 15466–15482.

25. Yuan, Q.; Cao, W.; Wang, X.-B. Cryogenic and Temperature-Dependent Photoelectron Spectroscopy of Metal Complexes. *Int. Rev. Phys. Chem*. **2020**, *39*, 83–108.

26. Hanstorp, D.; Gustafsson, M. Determination of the Electron Affinity of Iodine. *J. Phys. B: At., Mol. Opt. Phys*. **1992**, *25*, 1773–1783.

27. Wang, X.-B.; Wang, Y.-L.; Yang, J.; Xing, X.-P.; Li, J.; Wang, L.-S. Evidence of Significant Covalent Bonding in $Au(CN)_2^-$. *J. Am. Chem. Soc*. **2009**, *131*, 16368–16370.

28. Zhao, Y.; Truhlar, D. G. How Well Can New-Generation Density Functionals Describe the Energetics of Bond-Dissociation Reactions Producing Radicals? *J. Phys. Chem. A* **2008**, *112*, 1095–1099.

29. Zhao, Y.; Truhlar, D. G. The M06 Suite of Density Functionals for Main Group Thermochemistry, Thermochemical Kinetics, Noncovalent Interactions, Excited States, and Transition Elements: Two New Functionals and Systematic Testing of Four M06-Class Functionals and 12 Other Functionals. *Theor. Chem. Acc*. **2008**, *120*, 215–241.

30. Zhao, Y.; Truhlar, D. G. Density Functionals with Broad Applicability in Chemistry. *Acc. Chem. Res.* **2008**, *41*, 157–167.

31. Dunning Jr, T. H. Gaussian Basis Sets for Use in Correlated Molecular Calculations. I. The Atoms Boron Through Neon and Hydrogen. *J. Chem. Phys*. **1989**, *90*, 1007–1023.

32. Chai, J. -D.; Head-Gordon, M. Long-Range Corrected Hybrid Density Functionals with Damped Atom-Atom Dispersion Corrections. *Phys. Chem. Chem. Phys.* **2008**, *10*, 6615–6620.

33. Purvis III, G. D.; Bartlett, R. J. A Full Coupled-Cluster Singles and Doubles Model: The Inclusion of Disconnected Triples. *J. Chem. Phys*. **1982**, *76*, 1910–1918.

34. Watts, J. D.; Bartlett, R. J. The Coupled-Cluster Single, Double, and Triple Excitation Model for Open-Shell Single Reference Functions. *J. Chem. Phys*. **1990**, *93*, 6104–6105.

35. Barone, V.; Cossi, M. Quantum Calculation of Molecular Energies and Energy Gradients in Solution by a Conductor Solvent Model. *J. Phys. Chem. A* **1998**, *102*, 1995–2001.

36. Cossi, M.; Rega, N.; Scalmani, G.; Barone, V. Energies, Structures, and Electronic Properties of Molecules in Solution with the C-PCM Solvation Model. *J. Comp. Chem.* **2003**, *24*, 669–681.

37. GaussView, Ver. 6, Dennington, R.; Keith, T.; Millam, J. Semichem Inc., Shawnee Mission, KS, 2016.

38. Mozhayskiy, V. A.; Krylov, A. I. *ezSpectrum*, http://iopenshell.usc.edu/downloads.

39. Lu, T.; Chen, F. Multiwfn: A Multifunctional Wavefunction Analyzer, *J. Comput. Chem.* **2012**, *33*, 580-592.

40. Radziemski, L. J.; Kaufman, V. Wavelengths, Energy Levels, and Analysis of Neutral Atomic Chlorine (Cl I). *J. Opt. Soc. Am*. **1969**, *59*, 424–443.

41. Berzinsh, U.; Gustafsson, M.; Hanstorp, D.; Klinkmüller, A.; Ljungblad, U.; Mårtensson-Pendrill, A. -M. Isotope Shift in the Electron Affinity of Chlorine, *Phys. Rev. A* **1995**, *51*, 231–238.

42. Cioslowski, J. A. New Population Analysis Based on Atomic Polar Tensors. *J. Am. Chem. Soc*. **1989**, *111*, 8333–8336.

43. Metz, R. B.; Kitsopoulos, T.; Weaver, A.; Neumark, D. M. Study of the Transition State Region in the Cl+HCl Reaction by Photoelectron Spectroscopy of $ClHCl^-$, *J. Chem. Phys*. **1988**, *88*, 1463–1465.

44. Linstrom, P. J. and Mallard, W. G., Eds., NIST Chemistry WebBook, NIST Standard Reference Database Number 69, National Institute of Standards and Technology, Gaithersburg MD, 20899 https://doi.org/10.18434/T4D303, (retrieved August 7, 2024).

Table of Content Graphic

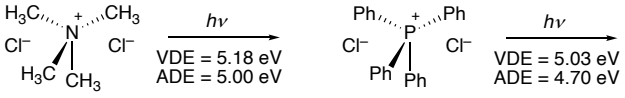

Ion Triplets Characterized by Photoelectron Spectroscopy